Determining aerosol particle size distributions using time-resolved laser-induced incandescence

Daun, Kyle J.; Stagg, B. J.; Liu, Fengshan; Smallwood, Gregory; Snelling, David

Publisher's version / Version de l'éditeur:

Proceedings of the ASME Heat and Transfer Division, 3, IMECE2006-13595, pp. 405-414, 2006

Proceedings of IMECE2006
2006 ASME International Mechanical Engineering Congress and Exposition
November 5-10, 2006, Chicago, Illinois, USA

IMECE2006-13595

DETERMINING AEROSOL PARTICLE SIZE DISTRIBUTIONS USING TIME-RESOLVED LASER-INDUCED INCANDESCENCE

K. J. Daun[1], B. J. Stagg[2], F. Liu[1], G. J. Smallwood[1], and D. R. Snelling[1]
[1]National Research Council of Canada, Ottawa, Canada, K1A 0R6
[2]Columbian Chemicals Company, 1800 West Oak Commons Ct., Marietta, GA 30062

ABSTRACT

Time-resolved laser-induced incandescence is a powerful tool for determining the physical characteristics of aerosol dispersions of refractory nano-particles. In this procedure, particles within a small aerosol volume are heated with a nano-second laser pulse, and the temporal incandescence of the particles is then measured as they return to the ambient gas temperature. It is possible to infer particle size distribution from the temporal decay of the LII signal since the cooling rate of an individual particle depends on its area-to-volume ratio. This requires solving a mathematically ill-posed inverse problem, however, since the measured LII signal is due to the incandescence contributed by all particle sizes within the aerosol volume.

This paper reviews techniques proposed in the literature for recovering particle size distributions from time-resolved LII data. The characteristics of this ill-posed problem are then discussed in detail, particularly the issues of solution stability and uniqueness. Finally, the accuracy and stability of each method is evaluated by performing a perturbation analysis, and the overall performance of the techniques is compared.

INTRODUCTION

The development of effective and accurate techniques for measuring particle size distributions in aerosols is important in many applications. For example, particle sizing is used to predict the impact of anthroporgenically-generated soot particles on human health [1] and the ecosystem [2]. Soot particle size also has a pronounced effect on radiation heat transfer in engines and furnaces [3], so determining particle morphology within these devices is paramount when optimizing their performance. Finally, accurate particle size measurement is crucial when manufacturing engineered nanoparticles [4].

Since its introduction by Melton [5], time-resolved laser-induced incandescence has become a powerful tool for making in-situ property measurements of aerosol dispersions, including the particle size distribution. In this procedure, a laser pulse heats a small volume of aerosol to temperatures substantially higher than the ambient gas temperature, typically 3000-3500 K in particle-sizing experiments. The particles then cool to the ambient gas temperature in microseconds, primarily by conduction to the surrounding gas. If sublimation and radiant heat loss effects are negligible, which is usually the case in low-fluence experiments, the particle temperature is governed by

$$\rho c \frac{\pi d_p^3}{6} \frac{dT_p(t, d_p)}{dt} = q_{in}(t, d_p) - q_{cond}(t, d_p), \qquad (1)$$

where $q_{in}(t, d_p)$ is the energy absorbed by the particle during the excitation laser pulse and $q_{cond}(t, d_p)$ is the conduction heat loss from the particle to the surrounding gas. If the excitation laser operates at a wavelength λ_e, the rate of laser energy absorption by the particle is given by

$$q_{in}(t, d_p) = F_0 \, q(t) \, Q_{abs,\lambda e}(d_p) \frac{\pi d_p^2}{4}, \qquad (2)$$

where F_0 is the total laser fluence and $q(t)$ is the pulsed laser temporal power density. If the particle absorbs in the Rayleigh limit ($\pi d_p/\lambda_e < 0.3$ [6]), the particle absorption efficiency is equal to $Q_{abs,\lambda e}(d_p) = 4\pi d_p/\lambda_e E(\boldsymbol{m}_{\lambda e})$, where $E(\boldsymbol{m}_{\lambda e})$ is the absorption function of the complex index of refraction. [Aggregated soot particles can also be modeled using Eq. (7), provided the primary particle diameters are within the Rayleigh limit [7].] At atmospheric pressures, heat conduction from the particle to the surrounding gas usually occurs within the free-molecular regime and is governed by [8]

$$q_{cond}(t, d_p) = \alpha_T \frac{\pi d_p^2}{4} \frac{P_g \bar{c}(T_g)}{2T_g} \frac{\gamma^* + 1}{\gamma^* - 1} \left[T_p(t, d_p) - T_g\right], \qquad (4)$$

where a_T is the thermal accommodation coefficient, γ^* is defined from

$$\frac{1}{\gamma^* - 1} = \frac{1}{T_p(t, d_p) - 1} \int_{T_g}^{T_p} \frac{dT}{\gamma(T) - 1}, \qquad (5)$$

and $\bar{c}(T_g) = \sqrt{8k_B T_g / \pi m_g}$. Equation (1) can be solved for the temperature of a particle of diameter d_p at any time t after the peak temperature. (Although aggregate shielding effects are important [9], they are neglected in this paper for simplicity.)

Because the particle cooling rate is inversely proportional to the particle volume-to-surface area ratio, the size distribution of particles in the measurement volume can be inferred from the incandescence decay rate. The spectral incandescence of the measurement volume at the detection wavelength λ is related to the particle temperatures through a Volterra integral equation of the first kind,

$$J_\lambda[t, f(d_p)] = C_\lambda \int_0^\infty f_d(d_p) K_\lambda(t, d_p) d\, d_p, \tag{6}$$

where $f(d_p)$ is the probability distribution function of the particle sizes and C_λ is a constant dependent on the particle volume fraction and the optical measurement system. The kernel of Eq. (6) is given by

$$K_\lambda(t, d_p) = E_{b,\lambda}(t, d_p)\, Q_{abs,\lambda}(d_p) \frac{\pi d_p^2}{4}, \tag{7}$$

where $E_{b,\lambda}(t, d_p)$ is the spectral emissive power of a blackbody at a temperature $T_p(t, d_p)$ and wavelength λ_i. Instead of relying on a single spectral incandescence measurement to determine the size distribution, many researchers measure the aerosol incandescence at two detection wavelengths and then calculate an effective temperature,

$$T_e[t, f_d(d_p)] = \frac{hc/k_B(1/\lambda_1 - 1/\lambda_2)}{\ln\left\{\frac{E(m_{\lambda 1})}{E(m_{\lambda 2})} \frac{J_{\lambda 2}[t, f_d(d_p)]}{J_{\lambda 1}[t, f_d(d_p)]} \left(\frac{\lambda_2}{\lambda_1}\right)^6\right\}}, \tag{8}$$

which is an implicit function of $f(d_p)$ through Eq. (7).

The spectral incandescence or effective temperature curve corresponding to a particular size distribution can be calculated directly from the above equations; we refer to this process as solving the mathematically well-posed *forward* problem. More often, however, the objective is to solve the *inverse* of this problem, i.e. to determine the size distribution that produced an experimentally-observed J_λ or T_e decay. This procedure is relatively straightforward if particle sizes are assumed to be monodisperse, in which case all particles have the same temperature decay curve and d_p is found directly from the time constant. This procedure was first used by Will et al. [10] and Mewes and Seitzman [11] to determine an average primary particle size of a soot aerosol using TR- LII measurements.

In reality, however, particle sizes in most aerosols are polydispserse and $f(d_p)$ can only be found by solving Eqs. (6) or (7). This is a far more difficult procedure because integral equations of the first-kind like Eq. (6) are mathematically ill-posed. The formal distinction between well-posed and ill-posed problems was first made by Hadamard [12], who defined well-posed problems as those that (i) have a solution (ii) that is unique and (iii) stable under small perturbations in the problem definition or input data; problems that fail to satisfy any of the above criteria are ill-posed. In this problem Hadamard's first criterion is satisfied since there must be at least one particle size distribution that produces the observed incandescence decay. There is, however, no guarantee that *only* one distribution produces the observed LII signal, at least within the resolution of the experimental apparatus. Furthermore, a particle size distribution that satisfies Eq. (7) may be very sensitive to small perturbations in the incandescence data and modeling errors. The latter is a particular concern, since many of the model parameters are not generally known with certainty.

The above properties make ill-posed problems very difficult to solve, so special mathematical techniques must be employed to recover the particle size distribution from time-resolved LII data. Mathematically ill-posed inverse problems can be solved in one of two ways: in the *explicit* methodology, the unknown parameter is usually solved for directly by first transforming the ill-posed governing integral equation into an ill-conditioned matrix equation that is then solved using regularization. Roth and Filippov [13] used this approach to solve Eq. (6) for $f(d_p)$ using an iterative regularization scheme [14, 15]. Although this method has been demonstrated on a test problem having a known distribution, it has limited practical utility since the maximum and minimum particle sizes must be known with some accuracy to restrict the null space of the coefficient matrix, and these values are rarely known for real aerosols.

In the *implicit* methodology, on the other hand, trial solutions of $f(d_p)$ are repeatedly substituted into the forward problem, either Eq. (6) or Eq. (8), until the modeled variable, $J_\lambda^{mod}(t)$ or $T_e^{mod}(t)$, matches experimentally-observed results within a specified tolerance. Lehre et al. [16, 17] were the first to use an implicit scheme to solve for the size distribution of a polydisperse aerosol using time-resolved LII data. Both Kuhlmann et al. [18] and Dankers and Leipertz [19] have also developed implicit techniques for finding particle size distributions using multivariate minimization. Liu et al. [20] developed an approach that transforms the multivariate minimization problem into an easier-to-solve univariate minimization problem.

This paper reviews the implicit methods that have been presented in the literature for finding the size distribution of polydisperse aerosols using time-resolved LII data. Each technique is described in detail and demonstrated by analyzing a set of artificial data generated using a specified size distribution. Finally, a discussion of how the ill-posed nature of the inverse problem affects the accuracy of the recovered size distributions is presented, and the resilience of each particle-sizing method to uncertainties in the model parameters and perturbations to the LII data is assessed.

TEST PROBLEM

The particle sizing techniques are demonstrated throughout this paper by using them to analyze an aerosol representative of

in-flame soot. The particle diameters follow a lognormal probability density function,

$$f_d(d_p) = \frac{1}{d_p \sqrt{2\pi} \ln \sigma_g} \exp\left[-\left(\frac{\ln d_p / d_{pg}}{\sqrt{2} \ln \sigma_g} \right)^2 \right], \quad (9)$$

and the corresponding cumulative distribution function

$$F_d(d_p) = \frac{1}{2}\left[1 + \text{erf}\left(\frac{\ln d_p / d_{pg}}{2 \ln \sigma_g} \right) \right], \quad (10)$$

which are plotted in Fig 1. The geometric mean, d_{pg}, and geometric standard deviation, σ_g, are set equal to 30 nm and 1.25, respectively, typical values for flame-generated soot primary particles [20].

The temperature of the spherical particles are calculated as they are heated from the ambient gas temperature, 1700 K, to a peak temperature of approximately 3300 K by the laser pulse and then cool back to the ambient gas temperature by solving Eq. (1) using a fourth-order Runge-Kutta scheme. The accommodation coefficient, α_T, is set equal to 0.3 and $E(m_\lambda)$ = 0.3 over all wavelengths. Temperature-dependent properties of soot and the flame gases are defined in a previous study [20].

The transient temperature distribution is then substituted into Eqs. (6-8) to obtain simulated spectral incandescence measurements at λ_1 = 400 nm and λ_2 = 780 nm along with the derived effective temperature, which are plotted in Fig. 2. (Simulated data for a monodisperse aerosol with d_p = 30 nm is also shown.) A sampling interval of two nanoseconds is assumed, which is typical of many experiments.

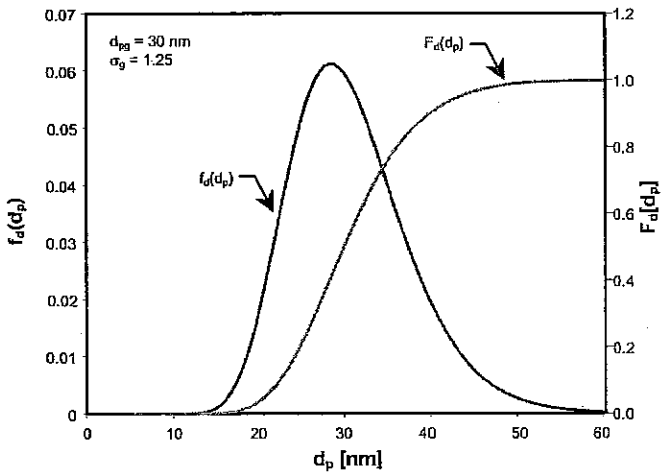

Fig. 1: Lognormal particle size distribution.

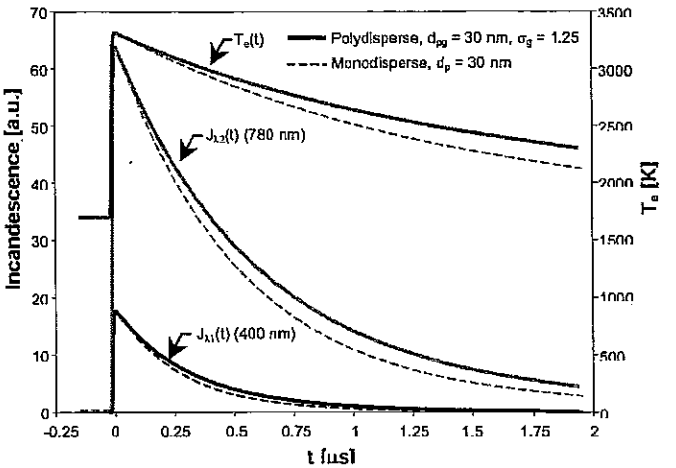

Fig. 2: Simulated incandescence and effective temperature data.

IMPLICIT SOLUTION SCHEMES

Implicit solution schemes work by repeatedly solving the well-posed forward problem, i.e. determining the incandescence intensity or effective temperature decay corresponding to trial particle size distributions, until the predicted quantity, either $J_\lambda^{mod}(t)$ or $T_e^{mod}(t)$, matches the experimentally-observed one. The most efficient way to do this is to recast the problem as a least-squares minimization problem,

$$\min_x [F(x)] = \min_x \left[\frac{1}{2} \left\| b^{exp} - b^{mod}(x) \right\|_2^2 \right], \quad (11)$$

where $F(x)$ is the objective function, the elements of x specify the particle size distribution, and vectors b^{exp} and $b^{mod}(x)$ contain experimentally-observed and modeled data. In aerosols containing soot the particle size distribution is most often assumed to be log-normal, so x is usually defined as $x \equiv \{d_{p,g}, \ln(\sigma_g)\}^T$. [Using $\ln(\sigma_g)$ instead of σ_g improves the scaling of the minimization problem.] Nonlinear programming is then used to find the value of x^* that satisfies $F(x^*) = \min[F(x)]$, which also defines the particle size distribution most likely to have produced the observed experimental data.

Many different nonlinear programming techniques have been developed to solve multivariate minimization problems like Eq. (11). These techniques minimize $F(x)$ iteratively; at the k^{th} iteration, the solution is updated by $x^{k+1} = x^k + p^k \alpha^k$ where p^k is a search direction and α^k is a step size, both of which are chosen based on the local topography of $F(x^k)$. If $F(x)$ is modeled accurately as a quadratic function in the vicinity of x^k, the most efficient choice for p^k is Newton's direction [21],

$$\nabla^2 F(x^k) p^k = -\nabla F(x^k), \quad (12)$$

where the gradient vector and Hessian matrix contain first- and second-order objective function sensitivities, $\nabla F_p(x^k)$ =

$\partial F(\boldsymbol{x}^k)/\partial x_p$ and $\nabla^2 F_{pq}(\boldsymbol{x}^k) = \partial^2 F(\boldsymbol{x}^k)/\partial x_p \partial x_q$, and α^k is set equal to unity. This approach, called Newton's method [21], usually requires the fewest iterations to find $\boldsymbol{x}$ of all the nonlinear programming methods, although the computational effort required to evaluate the second-order sensitivities make it unsuitable when $F(\boldsymbol{x})$ is expensive to calculate, which is the case in the present problem.

Instead, in most least-squares objective functions the Hessian is approximated accurately by $\nabla^2 F(\boldsymbol{x}^k) \approx \mathbf{J}^{\mathrm{T}}(\boldsymbol{x}^k)\mathbf{J}(\boldsymbol{x}^k)$ where $\mathbf{J}(\boldsymbol{x}^k)$ is the Jacobian of $f(\boldsymbol{x})$, $J_{pq}(\boldsymbol{x}^k) = -\partial^2 b^{mod}{}_p(\boldsymbol{x}^k)/\partial x_q$. Substituting this approximation for into Eq. (12) results in a procedure known as Gauss-Newton minimization [21], which is more computationally-efficient than Newton's method.

Unfortunately, in this problem both the Hessian and Jacobian matrices are ill-conditioned in the vicinity of $\boldsymbol{x}^*$ due to the ill-posedness of the underlying problem; consequently, while there exists a unique solution to Eq. (12), there are also a large set of search directions that almost satisfy Eq. (12) with a very small residual. The Levenburg-Marquardt method stabilizes the calculation of $\boldsymbol{p}^k$ by approximating the Hessian with $\nabla^2 F(\boldsymbol{x}^k) \approx \mathbf{J}^{\mathrm{T}}(\boldsymbol{x}^k)\mathbf{J}(\boldsymbol{x}^k) + \lambda^k \mathbf{I}$, where λ^k is a regularization parameter and $\mathbf{I}$ is the identity matrix. Although some implementations rely on the analyst to specify a satisfactory value of λ^k, most often the Levenburg-Marquardt method is implemented as a trust region method in which λ^k is specified implicitly through the size of the trust region, Δ^k, which forces $\|\boldsymbol{p}^k\|_2 \le \Delta^k$ at each iteration [22].

Although all implicit techniques work by solving a problem having the form of Eq. (12), each technique defines $F(\mathbf{x})$ in a different way. The first and most straightforward implementation by Lehre et al. [16], who defined $F(\mathbf{x})$ based on the difference between measured and modeled incandescence signals at m discrete observation times,

$$F(\boldsymbol{x}) = \frac{1}{2}\sum_{i=1}^{m}\left[J_\lambda^{exp}(t_i) - J_\lambda^{mod}(t_i,\boldsymbol{x})\right]^2. \qquad (13)$$

In a subsequent publication [17] effective temperature was substituted in place of monochromatic incandescence,

$$F(\boldsymbol{x}) = \frac{1}{2}\sum_{i=1}^{m}\left[T_e^{exp}(t_i) - T_e^{mod}(t_i,\boldsymbol{x})\right]^2. \qquad (14)$$

Equations (13) and (14) are plotted in Figs. 3 (*a*) and (*b*), respectively.

Kuhlmann et al. [18] developed a more sophisticated approach based on the method of cumulants. If a distribution $f(\Gamma)$ is related to a measured signal $g(t)$ through a Laplacian integral equation,

$$g(t) = \int_0^\infty f(\Gamma)\exp(-\Gamma t)\,d\Gamma, \qquad (15)$$

then the exponential decay of $g(t)$ can be expressed as a power-series of t,

$$\ln[g(t)] = -K_1 t + \frac{K_2 t^2}{2} + \ldots + \frac{K_n(-t)^n}{n!}, \qquad (16)$$

where the coefficients $\{K_i,\ i = 1, 2, \ldots\}$ are the cumulants of $f(\Gamma)$. If the distribution of Γ is log-normal, then $f(\Gamma)$ is defined completely by the first two cumulants, $2\sigma_g = K_2/K_1^2 + 1$ and $d_{pg} = K_1/2\sigma_g$. Unfortunately, this does not apply to Voterra integral equations of the first-kind in general, which can have more complicated kernels like Eq. (7). Instead, Kuhlmann et al. [18] derive cumulant-like parameters, K_1^{exp} and K_2^{exp}, from a quadratic regression of the log of experimentally-measured monochromatic incandescence signals, $\{\ln[J_\lambda^{exp}(t_i)]\}$, following Eq. (16). The least-squared objective function is then defined as

$$F(\boldsymbol{x}) = \frac{1}{2}\left\{\left[K_1^{exp} - K_1^{mod}(\boldsymbol{x})\right]^2 + \left[K_2^{exp} - K_2^{mod}(\boldsymbol{x})\right]^2\right\}, \qquad (17)$$

which is plotted in Fig. 3 (*c*).

Dankers and Leipertz [19] developed a similar method based on fitting two exponential curves to the monochromatic incandescence signal over two different time domains, Δt_1 and Δt_2. The first time domain starts approximately 100 ns after the laser pulse and lasts 150-200 ns, while Δt_2 typically starts at 600 ns and lasts 200 ns provided the particles are sufficiently large and the ambient gas temperature is high. The particle size distribution is then found by comparing the time constants of the exponential curves, t_1^{exp} and t_2^{exp}, to databases of model-generated time constants formed by varying d_{pg} and σ_g over a range of values. This is equivalent to minimizing

$$F(\boldsymbol{x}) = \frac{1}{2}\left\{\left[\tau_1^{exp} - \tau_1^{mod}(\boldsymbol{x})\right]^2 + \left[\tau_2^{exp} - \tau_2^{mod}(\boldsymbol{x})\right]^2\right\}, \qquad (18)$$

which is plotted in Fig. 3 (*d*).

Although all the above implicit methods minimize different objective functions, Fig. 3 shows that these functions all feature a long, shallow valley surrounding a strong local minimum at $\boldsymbol{x}^*$. This topography is due to the fundamental nature of the ill-posed problem; each objective function has at least one minimizer $\boldsymbol{x}^*$, so Hadamard's first criterion requiring the existence of at least one solution is satisfied. Furthermore, the objective functions have only one minimizer [at least over the plotted range of d_{pg} and $\ln(\sigma_g)$], which means that Hadamard's second criterion demanding solution uniqueness is also satisfied. The problem is ill-posed because any point $\tilde{\boldsymbol{x}}^*$ along the floor of the valley surrounding $\boldsymbol{x}^*$ specifies a particle size distribution that *almost* minimizes $F(\boldsymbol{x})$, i.e. it produces modeled TR-LII data that closely resembles the experimentally observed data, even though $\tilde{\boldsymbol{x}}^*$ and $\boldsymbol{x}^*$ specify completely different distributions. Because of this, Hadamard's second criterion is *almost* violated, and as we will show later in the paper, Hadamard's third criterion is violated.

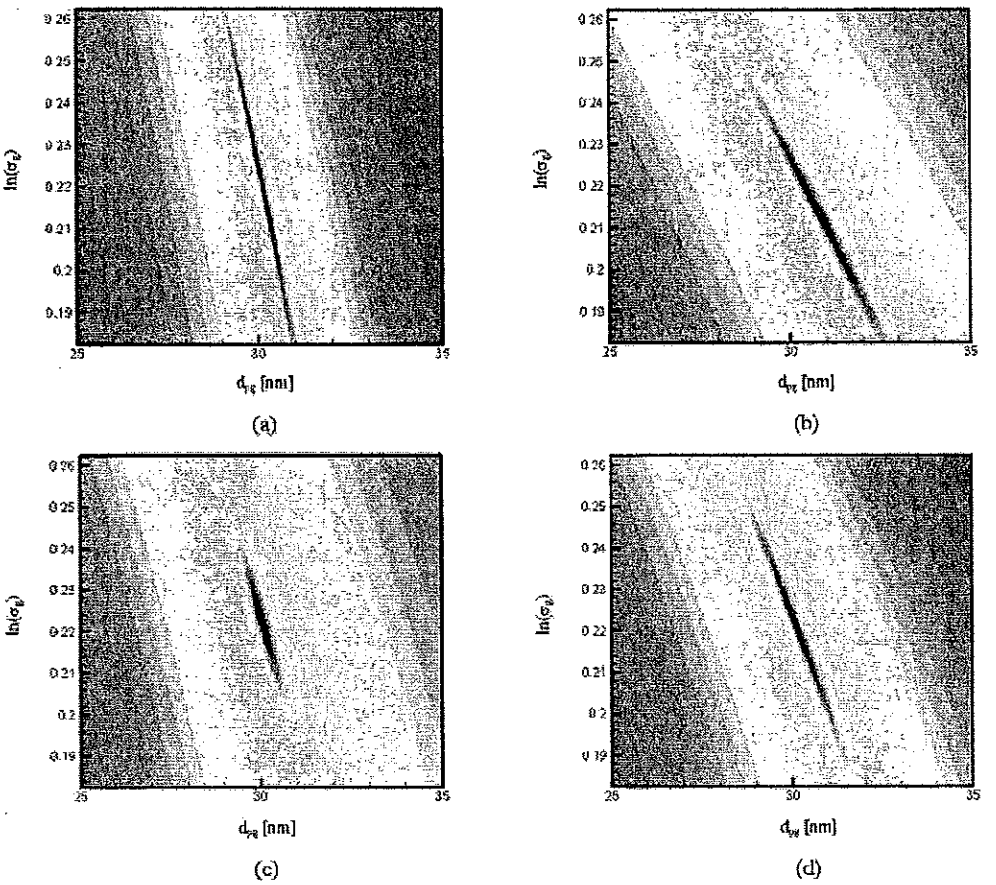

Fig 3: Plots of Least-squares objective functions for different implicit solution techniques (a) Eq. (13), (b) Eq. (14), (c) Eq. (17) and (d) Eq. (18). Objective functions are normalized and plotted on an exponential scale.

A technique proposed by Liu et al. [20] further elucidates the ill-posed nature of the problem. It is based on the observation that, if the particles are heated to the same peak temperature at t_{max}, the initial effective temperature decay rate is governed by

$$\left.\frac{d\ln\left(T_e - T_g\right)}{dt}\right|_{t_{max}} = -\frac{C}{d_{p32}}, \tag{19}$$

where

$$C = \frac{3}{4}\frac{\alpha_T}{\rho c}\frac{P_g \bar{c}}{T_g}\left(\frac{\gamma^* + 1}{\gamma^* - 1}\right), \tag{20}$$

and d_{p32} is the Sauter mean diameter,

$$d_{p32} = \int_0^\infty f\left(d_p\right) d_p^3 \, d\, d_p \Big/ \int_0^\infty f\left(d_p\right) d_p^2 \, d\, d_p, \tag{21}$$

which for a lognormal distribution is equal to

$$d_{p32} = d_{pg} \exp\left[5/2 \ln\left(\sigma_g\right)^2\right]. \tag{22}$$

Equations (19)-(21) provide a relationship between σ_g and d_{pg} and show that particle size distributions having the same Sauter mean diameter also have the same initial effective temperature decay after the laser pulse. At later times in the cooling process, however, the effective temperature decay rate becomes unique to a particular particle size distribution. In this approach, the first step is to calculate d_{p32} by performing a linear regression on a set of $\{\ln[T_e^{exp}(t_i)-T_g]\}$ data, where $t_{max} \le t_i \le t_{max} + 100$ ns. Once d_{p32} has been found, the lognormal size distribution is specified by only one parameter, say σ_g. The next step is to find the value of σ_g that causes the modeled effective temperature to match the measured effective temperature at some time t_c after the peak soot temperature, which can be done by minimizing

$$F\left(\sigma_g\right) = \left[T_e^{exp}\left(t_c\right) - T_e^{mod}\left(t_c, \sigma_g\right)\right]^2. \tag{23}$$

Liu et al. [20] found that the maximum sensitivity of $T_e(t_c)$ to σ_g was found by setting t_c = 1.5 μs. Figure 4 shows the curve $d_{32} = d_{pg}\exp[5/2\ln(\sigma_g)^2]$ plotted over the topography of Eq. (14) generated with $J_\lambda^{exp}(t_i)$ data collected between t_{max} and t_{max} +

100 ns. Note that the Sauter mean curve corresponds to the floor of the valley surrounding x^*, since different size distributions having the same d_{p32} produce similar incandescence curves. This is *almost* a violation of Hadamard's second criteria and causes a violation of Hadamard's third criterion, which is demonstrated in the next section.

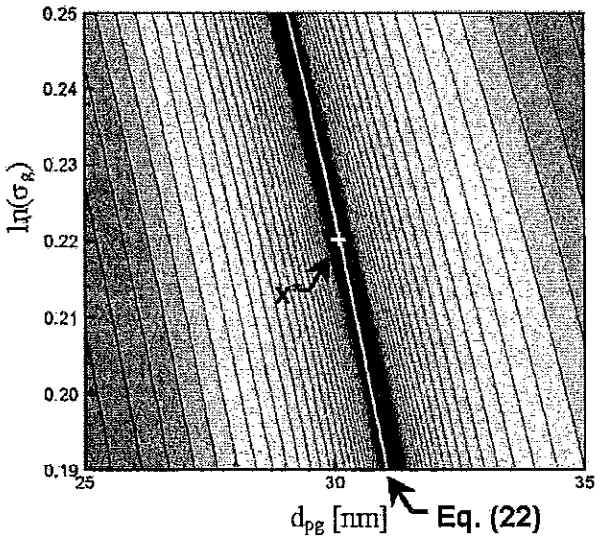

Fig. 4: Eq. (22) plotted over Eq. (14), generated using data measured up to 100 ns after the laser pulse.

SOLUTION ACCURACY AND STABILITY

In the previous section we showed particle sizing through inverse analysis of time-resolved LII data requires the solution of an ill-posed problem that violates Hadamard's third criteria, i.e. that the recovered solution is highly sensitive to perturbations to the problem definition. In this problem, the perturbations are due to uncertainties in the model parameters and noise in the measured data.

Model Parameter Uncertainty

Many of the model parameters in time-resolved laser-induced incandescence studies are not known with a high degree of certainty, as recently highlighted by Schulz et al. [23] amongst others. In particular, the majority of LII studies on in-flame soot in the recent literature report values of α_T ranging from 0.23 to 0.37 [24] and wavelength-averaged values of $E(m)$ that range from 0.2 to 0.4 [25]. Lehre et al. [17] also suggest that particle sizing is sensitive to errors in gas temperature measurement; the accuracy of T_g depends on how it is measured, but even the most accurate in-flame measurement techniques are subject to measurement uncertainties of at least 5%. (The uncertainties of high-fluence LII are manifold and are not discussed here.)

The relative sensitivity of the size distributions recovered by the implicit techniques described above to model parameter uncertainties is assessed by performing a perturbation analysis. In this procedure, artificial monochromatic and dichromatic incandescence is first generated using the nominal model parameters, $\alpha_T = 0.3$, $E(m) = 0.3$, and $T_g = 1700$ K, and the particle size distribution shown in Fig. 1. The five implicit techniques are then used to recover the particle size distribution from these artificial data sets, except the model parameters are perturbed to maximum and minimum values representative of the parameter uncertainties summarized in Table 1. In each case, the accuracy of the recovered distribution is quantified by the Cramér-Von Mises (CVM) goodness-of-fit parameter [26], defined as the area contained between the recovered and exact particle size cumulative distribution functions,

$$[W(x)]^2 = \int_0^\infty \left[F_d(d_p, x) - F_d(d_p, x^*)\right]^2 d\,d_p, \quad (24)$$

which is shown graphically in Fig. 5.

Table 1: Nominal model parameters and perturbations.

Model Parameter	Nominal Value	Perturbation
α_T	0.3	± 0.05
$E(m)$	0.3	± 0.1
T_g	1700 K	± 20 K

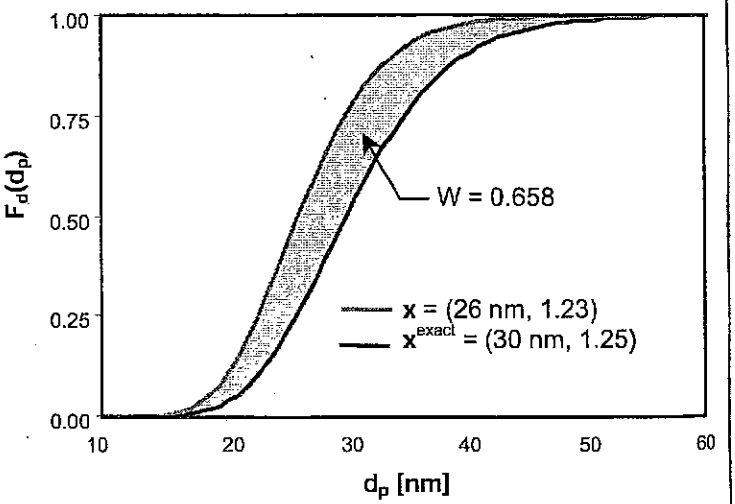

Fig. 5: Graphical representation of the Cramér-Von Mises goodness-of-fit statistic.

The maximum CVM statistic associated with each perturbation is summarized in Table 2. The first column shows the CVM statistics of the unperturbed recovered distributions, which are slightly larger than zero because the cooling models neglect residual laser heating after the peak temperature. Table 2 shows that the implicit schemes are most sensitive to accommodation coefficient uncertainties and are relatively insensitive to uncertainties in $E(m)$ and T_g. In fact, methods based on two-wavelength pyrometry are completely insensitive

to $E(m)$ if it is truly wavelength-independent. Figure 6 shows the particle size distributions recovered using Eq. (14) with perturbed accommodation coefficient values.

The above observations assume that the peak particle temperature is measured using two-color pyrometry, Eq. (8). Alternatively, one can avoid two-color measurements and instead estimate the peak temperature by solving Eq. (1), which is sometimes done with techniques that otherwise rely only on monochromatic incandescence measurements. The CVM statistics associated with this technique are included parenthetically in the $E(m)$ column, and show that it is highly sensitive to uncertainties in $E(m)$.

Table 2: Maximum CVM statistics due to model parameter uncertainty.

Method	Nominal	$\alpha_T \pm 0.05$	$T_g \pm 20$ K	$E(m) \pm 0.1$
Ref. [16]	0.021	1.206	0.179	0.021 (2.578)
Ref. [17]	0.168	1.165	0.241	0.168
Ref. [18]	0.010	1.058	0.073	0.010 (0.843)
Ref. [19]	0.013	1.055	0.068	0.013 (1.153)
Ref. [20]	0.305	1.311	0.385	0.305

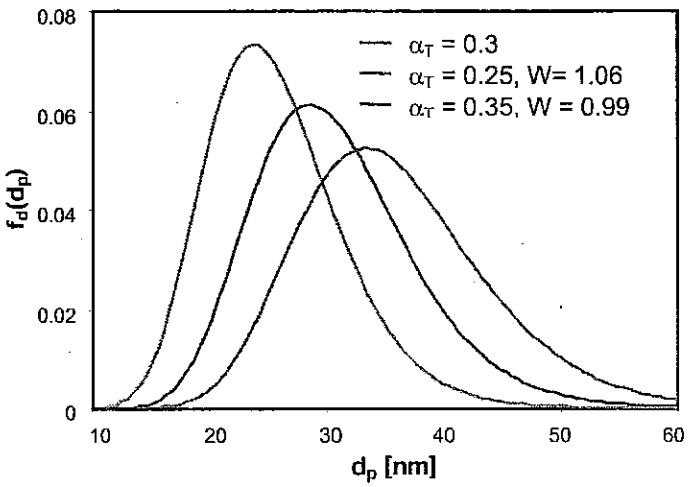

Fig. 6: Effect of α_T uncertainty on size distributions recovered with the method of Lehre et al. [17]

Measurement Noise

In order to assess the sensitivity of the implicit solution methods to measurement noise, the synthetic incandescence data was contaminated with artificial photomultiplier shot noise according to

$$\tilde{J}_\lambda(t_i) = J_\lambda(t_i) + \varepsilon_\lambda(t_i). \qquad (25)$$

The time-dependent error, $\varepsilon_\lambda(t_i)$, is sampled from an unbiased Gaussian distribution having a standard deviation of $K_\lambda / \sqrt{N_{shots}\, J_\lambda(t_i)}$, which is consistent with the operating theory of photodetectors [27]. In this work, K_λ is set equal to five percent of the maximum signal strength and N_{shots} represents the number of single-shot measurements used for variance reduction. The simulated 10-shot averaged LII data plotted in Fig. 7 shows that signals collected at short wavelengths are most susceptible to noise and that the signal-to-noise ratio increases with time, which are both characteristic of experimental data. Figure 7 also shows that calculating an effective temperature using two-wavelength pyrometry amplifies the experimental noise substantially, as observed by Kuhlmann et al. [18].

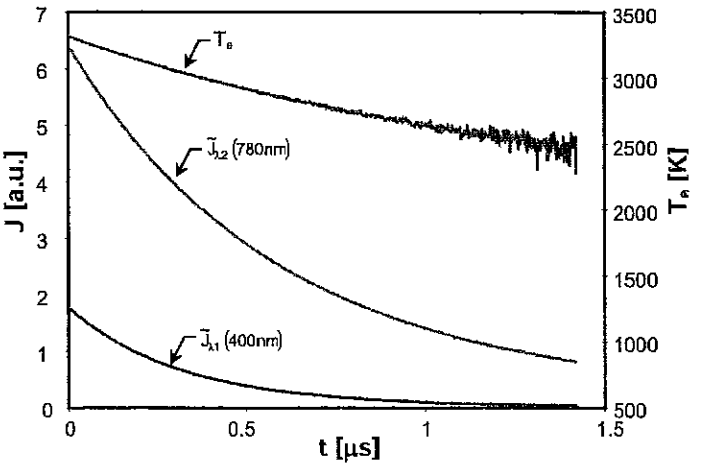

Fig. 7: Synthetic 10-shot averaged LII data

The influence of objective function topography on error propagation is demonstrated in Fig. 8, which shows 40 solutions recovered from perturbed 10-shot averaged LII data using the method of Kuhlmann et al. [18] and plotted over the contours of the corresponding objective function. All the solutions lie in the vicinity of the shallow valley surrounding x^*, a topographical feature characteristic of ill-posed problems that violate Hadamard's third criterion, since solutions that lie in this valley almost minimize $F(\mathbf{x})$ and produce modeled LII signals that closely resemble the unperturbed LII signal corresponding to the true distribution. The locus of solutions is slightly skewed from the valley of the objective function, however, because the measurement noise biased towards longer cooling times. The perturbed solutions actually follow the locus of distributions having the same Sauter mean diameter, since this value depends only on the initial rate of cooling and the corresponding data is relatively unperturbed.

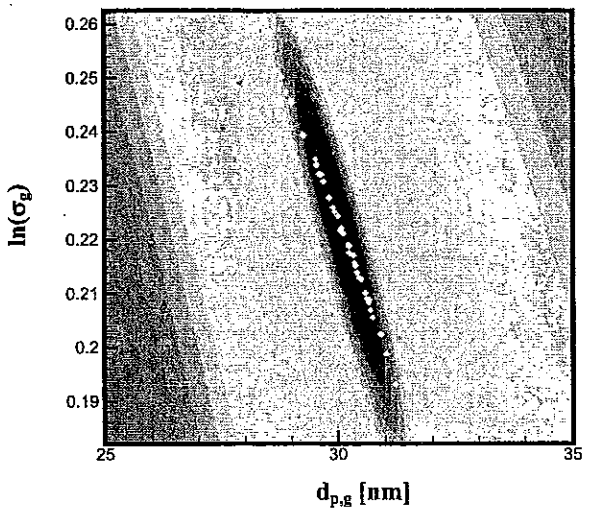

Fig. 8: Solutions obtained using the Kuhlmann et al. method [18] on perturbed 10-shot data, plotted over the corresponding objective function contours.

The sensitivity of the implicit sizing techniques to measurement noise is compared by using them to recover size distributions from 40 independent sets of incandescence data contaminated with artificial noise, and with different values of N_{shots} for variance reduction. The average CVM parameters are plotted in Fig. 9, and show that techniques based on monochromatic incandescence are less susceptible to measurement noise compared to those based on effective temperature. The different sensitivities of the implicit sizing techniques to measurement noise has little to do with the relative objective function topography, and instead depends on noise amplification caused by the derived variables that define the least-squares objective function. Figure 10 shows that while there is very minor noise amplification associated with the parameters of the Kuhlmann et al. method [18] and the Dankers and Leipertz method [19], substantial noise amplification occurs when using methods based on effective temperature. The method of Liu et al. [24] is most sensitive to measurement noise because Eq. (23) is derived using only on a single effective temperature; in contrast, Eq. (14) relies on a large set of effective temperatures, which somewhat mitigates the noise in the effective temperature data.

CONCLUSIONS

This paper has shown that using time-resolved LII data to recover the particle distribution in an aerosol involves solving an ill-posed inverse problem that violates Hadamard's third criterion. Although both explicit and implicit solution techniques have been proposed in the literature, implicit solution techniques based on least-squares minimization are the most viable way of solving this problem.

Because the problem is ill-posed, the recovered particle size distribution is sensitive to both model parameter uncertainty and measurement noise. All implicit methods are roughly equally sensitive to uncertainties in the model parameters, the thermal accommodation coefficient in particular. Techniques based on monochromatic incandescence are least susceptible to measurement noise.

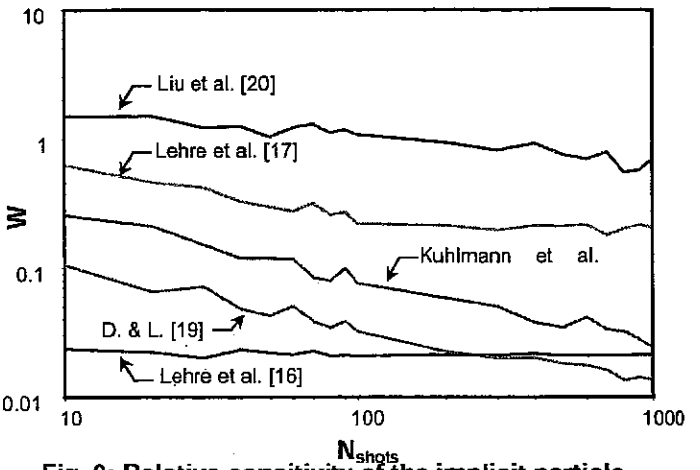

Fig. 9: Relative sensitivity of the implicit particle sizing techniques to measurement noise.

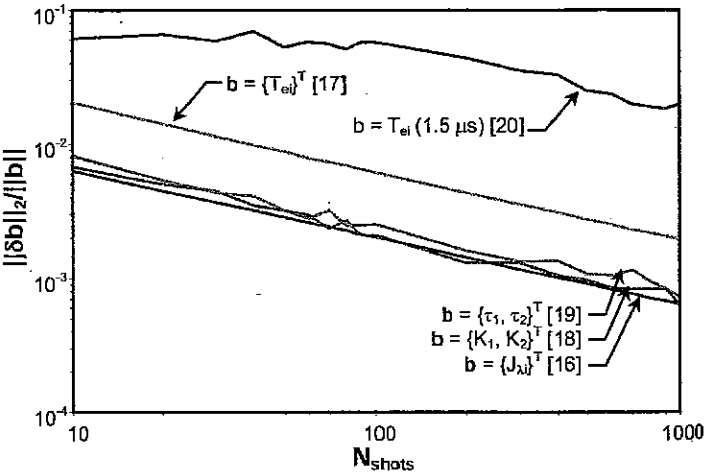

Fig. 10: Noise amplification caused by the derived least-squared objective function variables.

NOMENCLATURE

b^{exp}	Vector containing experimentally-measured data
$b^{mod}(x)$	Vector containing modeled data
c	Specific heat, J/kgK
$\bar{c}$	Mean molecular speed, ms^{-1}
C_λ	Calibration constant
d_p	Particle diameter, m
d_{pg}	Geometric mean particle diameter, m
d_{p32}	Sauter mean diameter, Eq. (21), m
$E_{b\lambda}(t, d_p)$	Spectral emissive power of particles having diameter d_p
$E(m_\lambda)$	Absorption function of the complex index of refraction.
$f_d(d_p)$	Probability density function of d_p
$F_d(d_p)$	Cumulative distribution function of d_p
$F(x)$	Least-squares objective function
$\mathbf{I}$	Identity matrix
$J_\lambda(t)$	Monochromatic incandescence signal
$\mathbf{J}(x^k)$	Jacobian matrix of $F(x)$
k_B	Boltzmann's constant, 1.38×10^{-23} $J/molecule\ K$
$K_\lambda(t, d_p)$	Kernel of Eq. (7)
m_g	Molecular mass of the gas, kg
N_{shots}	Number of single-shot measurements for variance reduction
p^k	Search direction
$Q_{abs,\lambda}(d_p)$	Absorption efficiency of particles having a diameter d_p
t	Time, s
$T_e(t)$	Effective temperature, K
T_g	Gas temperature, K
$T_p(d_p, t)$	Particle temperature, K
W	Cramér-Von Mises parameter, Eq. (24)
x	Vector specifying $f_d(d_p)$
α_T	Thermal accommodation coefficient
α^k	Step size
Δ^k	Trust region size
$\varepsilon_\lambda(t)$	Synthetic measurement noise
γ^*	Temperature-averaged adiabatic gas constant
λ_e	Laser excitation wavelength
λ_1	First detection wavelength, 400 nm
λ_2	Second detection wavelength, 780 nm
λ^k	Regularization parameter
ρ	Density, kg/m^3
σ_g	Geometric standard deviation

REFERENCES

[1] Oberdörster, G., Oberdörster, E., and Oberdörster, J., 2005, "Nanotoxicology: An Emerging Discipline Evolving from Studies of Ultrafine Particles," Environmental Health Perspectives, **113**, 7, pp. 823-839.

[2] Jacobson, M. Z., 2002, "Control of Fossil-Fuel Particulate Carbon Black and Organic Matter, Possibly the Most Effective Method of Slowing Global Warming," J. Geophysical Research, **107**, D19.

[3] Viskanta, R., and Menguç, M. P., 1987, "Radiation Heat Transfer in Combustion Systems," Progress in Energy and Combustion Science, **13**, 2, pp. 97-160.

[4] Dankers, S., Leipertz, A., Will, S., Arndt, J., Vogel, K., Schraml, S., Hemm, A., 2003, "In-situ Measurement of Primary Particle Sizes during Carbon Black Production," Chemical Engineering Technology, **26**, 9, pp. 966-969.

[5] Melton, L. A., 1984, "Soot Diagnostics based on Laser Heating," Applied Optics, **23**, 13, pp. 2202-2208.

[6] Kerker, M, The Scattering of Light, Academic Press, New York, NY, 1969.

[7] Farias, T. L., Köylu, Ü. Ö., and Carvalho, M. G., 1996, "Range of Validity of the Rayleigh-Debye Gans Theory for Optics of Fractal Aggregates," Applied Optics, **35**, 33, pp. 6560-6567.

[8] Filippov, A. V., and Rosner, D. E., 2000, "Energy Transfer between an Aerosol Particle and Gas at High Temperature Ratios in the Knudsen Transition Regime," IJHMT, **43**, 12, pp. 127-138.

[9] Filippov, A. V., Zurita, M., and Rosner, D. E., 2000, "Fractal-like Aggregates: Relation between Morphology and Physical Properties," J. Colloid Interface Sci., **229**, 1 pp. 261-273.

[10] Will, S., Schraml, S., and Leipertz, A. 1995, "Two-Dimensional Soot-Particle Sizing by Time-Resolved Laser-Induced Incandescence," Optical Letters, **20** 22, pp. 2341-2344.

[11] Mewes, B., and Seitzman, J. M., 1997, "Soot Volume Fraction and Particle Size Measurements with Laser-Induced Incandescence," Applied Optics, **36**, 3, pp. 709-717.

[12] Hadamard, J., 1923, Lectures on Cauchy's Problem in Linear Partial Differential Equations, Yale University Press, New Haven, CT.

[13] Roth, P., and Filippov, A. V., 1996, "In Situ Ultrafine Particle Sizing by a Combination of Pulsed Laser Heatup and Particle Thermal Emission," J. Aerosol Sci., **27**, 1, pp. 95-104.

[14] Twomey, S. 1975, "Comparison of Constrained Linear Inversion and an Iterative Nonlinear Algorithm Applied to the Indirect Estimate of Particle Size Distributions," J. Computational Physics, **18**, pp. 188-200.

[15] Markowski, G. R., 1987, "Improving Twomey's Algorithm for Inversion of Aerosol Measurement Data," Aerosol Sci. and Tech., 7, 2, pp. 127-141.

[16] Lehre, T. Bockhorn, H., Jungfleisch, B., and Suntz, R., 2003, "Development of a Measuring Technique for Simultaneous In Situ Detection of Nanoscaled Particle Size Distributions and Gas Temperatures," Chemosphere, **51**, 10, pp. 1055-1061.

[17] Lehre, T. Jungfleisch, B., Suntz, R., and Bockhorn, H. 2003, "Size Distributions of Nanoscaled Particles and Gas Temperatures from Time-Resolved Laser-Induced Incandescence Measurements," Applied Optics, 42, 12, pp. 2021-2029.

[18] Kuhlmann, S. A., Schumacher, J., Reimann, J., and Will, S., 2004, "Evaluation and Improvement of Laser-Induced Incandescence for Nanoparticle Sizing," PARTEC 2004, Nuremburg, Germany, March 16-18.

[19] Dankers, S. and Leipertz, A., 2004, "Determination of Primary Particle Size Distributions from Time-Resolved Laser-Induced Incandescence Measurements," Applied Optics, **43**, 138, pp. 3726-3730.

[20] Liu, F., Stagg, B. J., Snelling, D. R., and Smallwood, G. J., 2006, "Effects of Primary Soot Particle Size Distribution on the Temperature of Soot Particles Heated by a Nanosecond Pulsed Laser in an Atmospheric Laminar Diffusion Flame." IJHMT, **49**. pp. 777-788.

[21] Gill, P. E., Murray, W., Wright, M. H., 1986, Practical Optimization, Academic Press, San Diego, CA.

[22] More, J. J., and Sorensen, D. C., 1983, "Computing a Trust Region Step," SIAM J. Sci. Statist. Comput. **4**, 3, pp. 553-572.

[23] Schulz, C., Kock, B. F., Hofmann, M., Michelsen, H., Will, S., Bougie, B., Suntz, R., and Smallwood, G. J., 2006, "Laser-Induced Incandescence: Recent Trends and Current Questions," Applied Physics B, **83**, 3, pp. 333-354.

[24] Liu, F., Snelling, D. R., and Smallwood, G. J., 2006, "A Critical Evaluation of the Thermal Accommodation Coefficient of Soot Determined by the Laser-Induced Incandescence Technique," 13th IHTC, Sydney, Australia, Aug. 13-18.

[25] Liu, F. Daun, K. J., and Smallwood, G. J., 2006, "Some Theoretical Considerations for Modeling Laser-Induced Incandescence at Small Pressures," 2nd Intl. Bunsen Meeting and Workshop, Bad Herrenalb, Germany, Aug. 2-4.

[26] Stephens, M. A., 1970, "Use of the Kolmogorov-Smirnov, Cramer-Von Mises and Related Statistics Without Extensive Tables," J. Royal Statistical Soc. B, **32**, 1, pp. 115-122.

[27] Yariv, A., 1971, Introduction to Optical Electronics, Holt, Reinhold and Winston, Inc., New York, NY, pp. 254-256.

HTD-Vol. 377-3

Proceedings of the ASME

HEAT TRANSFER DIVISION
– 2006 –

VOLUME 3

HEAT TRANSFER IN ELECTRONIC EQUIPMENT
LOW TEMPERATURE
ENVIRONMENTAL HEAT TRANSFER
COMPUTATIONAL HEAT TRANSFER
EDUCATION
VISUALIZATION OF HEAT TRANSFER

presented at
2006 ASME INTERNATIONAL MECHANICAL ENGINEERING CONGRESS AND EXPOSITION
NOVEMBER 5–10, 2006
CHICAGO, ILINOIS USA

sponsored by
THE HEAT TRANSFER DIVISION, ASME

A S M E
Three Park Avenue ◆ New York, N.Y. 10016